

An Improved Random Path Length Algorithm for p-i-n and Staircase Avalanche Photodiodes

Alessandro Pilotto*, Pierpaolo Palestri*, Luca Selmi†, Matias Antonelli‡, Fulvia Arfelli§¶, Giorgio Biasiol||, Giuseppe Cautero‡¶, Francesco Driussi*, Ralf H. Menk‡¶**, Camilla Nichetti‡§, Tereza Steinhartova§||

*DPIA, University of Udine, 33100 Udine, Italy. Email: pilotto.alessandro@spes.uniud.it

†DIEF, University of Modena and Reggio Emilia, 44100 Modena, Italy.

‡Elettra-Sincrotrone Trieste S.C.p.A, Area Science Park Basovizza, 34149 Trieste, Italy.

§Department of Physics, University of Trieste, 34128 Trieste, Italy.

¶Istituto Nazionale di Fisica Nucleare, INFN Sezione di Trieste, Trieste, 34100, Italy.

||IOM CNR, Laboratorio TASC, Area Science Park Basovizza, 34149 Trieste, Italy.

**Department of Medical Imaging, University of Saskatchewan, Saskatoon, SK S7N 5A2, Canada.

Abstract—We present an improved Random Path Length algorithm to accurately and efficiently estimate the design space of heterostructure avalanche photodiodes (APDs) in terms of gain, noise and bandwidth without any need of full Monte Carlo transport simulations. The underlying nonlocal model for impact ionization goes beyond the Dead Space concept and it is suited to handle staircase structures composed by a superlattice of III-V compounds as well as thick and thin p-i-n APDs. The model parameters have been calibrated on GaAs and Al_xGa_{1-x}As p-i-n APDs in a previous work. In this work GaAs p-i-n APDs are compared to staircase structures in terms of noise and bandwidth.

Index Terms—Staircase APDs, Random Path Length, Impact Ionization, Avalanche Multiplication, Excess Noise Factor, Bandwidth, Simulation.

I. INTRODUCTION

Avalanche photodiodes (APDs) working in the linear regime (i.e. below breakdown, as opposed to Geiger mode operation) find widespread use in optical fiber links and in single photon detectors. The internal gain provided by impact ionization (II), however, adds multiplication noise. Adequate models are necessary to design APDs to operate in the “sweet spot” of the gain, noise [1] and bandwidth [2] space. The local model of [1], [2] is inadequate to this purpose if applied to thin p-i-n diodes or to complex staircase structures [3]. Nonlocal history-dependent models based on the Dead Space approach [4] or on the concept of effective fields [5] have been proposed. Recently, [6] proposed the following alternative definition of the effective fields, derived from a simple energy balance equation which is suited also for staircase structures:

$$E_{eff,e}(x|x') = \frac{1}{\lambda_e} \int_x^{x'} \frac{dE_C}{dx}(x'') \exp\left(\frac{x'' - x'}{\lambda_e}\right) dx''. \quad (1)$$

A similar effective field $E_{eff,h}(x|x')$ is defined also for holes. Here x' is the position where II takes place for a carrier generated optically or by II at position x . E_C (and E_V needed for the hole effective field) are the conduction and valence

band profiles and λ_e (plus λ_h) suitable mean free paths. The E_C and E_V profiles are obtained from TCAD simulations [7] assuming that the photo-generated current has a negligible effect on the electrostatics of the device. The nonlocal II coefficients are then calculated from the effective fields:

$$\alpha(x|x') = A_e \cdot \exp\left[-\left(\frac{E_{ce}}{E_{eff,e}(x|x')}\right)^{\gamma_e}\right], \quad (2)$$

where A_e , E_{ce} , and γ_e are adjustable model parameters. Similarly it is done for the hole II coefficient $\beta(x|x')$. The models in [4]–[6] use $\alpha(x|x')$ and $\beta(x|x')$ to derive the spatial distribution of the carriers generated by II: the probability that an electron that starts its motion at x has its first ionizing collision in the interval $[x', x' + dx']$ is given by

$$p_e(x|x')dx' = \alpha(x|x') \exp\left(-\int_x^{x'} \alpha(x|x'')dx''\right) dx'. \quad (3)$$

The probability that an electron does not suffer an ionizing collision in the $[x, x']$ interval is therefore given by

$$P_{se}(x|x') = \exp\left(-\int_x^{x'} \alpha(x|x'')dx''\right). \quad (4)$$

If we denote as $x = 0$ and $x = W$ the boundaries of the multiplication region, then the average number of carriers generated by the II of an electron injected at x (including itself) can be expressed as

$$N_e(x) = P_{se}(x|W) + \int_x^W [2N_e(x') + N_h(x')] \times \alpha(x|x') P_{se}(x|x') dx'. \quad (5)$$

Similar equations are used to determine the average number of carriers generated by the II of a hole $N_h(x)$ and the standard deviations of these quantities. This results in a system of equations (either integral [4], [5] or algebraic [6]) which gives the gain and the noise for an e-h pair generated at position x .

However, the dynamics of the process is not described, so that the actual current waveform and the corresponding device bandwidth cannot be determined. A more complex system of

This work was supported by Italian MIUR through the PRIN 2015 Project under Grant 2015WMZ5C8.

recursive equations has been proposed in [8] to obtain the waveforms in the framework of the Dead Space approach, but the application to the nonlocal models in [5] and [6] is not straightforward.

II. MODEL DESCRIPTION

A powerful alternative to the models in [4]–[6] is the Random Path Length (RPL) algorithm [9]: the distance travelled by a carrier between two II events is determined randomly; secondary carriers are generated and undergo the same process until they exit from the simulation domain. In [9] the path between two II events is computed by adding the dead space length to a random length related to α (assumed to depend only on the local field). In this paper we go beyond this simple approach and use (1)–(2), thus extending the model validity to structures with heterojunctions, band offsets and non-uniform electric field profiles.

Following (3) and (4), the distance travelled by an electron after generation at the position x can be determined by generating a random number r , uniformly distributed in $[0, 1]$ and finding x' by inverting (numerically) the condition:

$$r = P_{se}(x|x') = \exp\left(-\int_x^{x'} \alpha(x|x'') dx''\right). \quad (6)$$

The time associated with this displacement is $(x' - x)/v_e$, where v_e is the average velocity. Similar equations hold for holes. At position x' we then generate another e-h pair. Recursive functions are used to handle the increased number of carriers in the simulations as in [10], meaning that carriers are kept in the stack until they exit from the simulation domain.

By repeating the stochastic algorithm described above many times (starting with the initial e-h pair at position x) one can extract the average gain $M = \langle m \rangle$ (m being the gain obtained in a sample sequence) and the excess noise factor $F = \langle m^2 \rangle / M^2$. At the same time, by using Ramo's theorem [11] we can determine the current pulse amplitude due to an electron moving from x to x' as illustrated in Fig. 1.

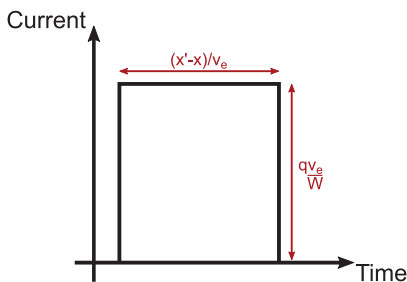


Fig. 1. Contribution of a single electron travelling from x to x' with average velocity v_e to the total current waveform. The term $1/W$ is an approximation of dE/dV which is prescribed by Ramo's theorem [11], where E is the local electric field and V is the applied bias voltage.

Although the RPL is a Monte Carlo technique, it should not be confused with the commonly used Monte Carlo method for carrier transport simulation in electronic devices [12]. In fact, the RPL algorithm embeds scattering rates and band structure

information into average ionization probability per unit length (α) and average carrier velocity (v_e) [13]. The computational burden is orders of magnitude smaller than for Monte Carlo device simulation, but this comes at the expense of accuracy.

III. RESULTS

A. Gain and noise in GaAs p-i-n APDs

As far as gain and noise are concerned, the RPL algorithm should give exactly the same results as the deterministic approaches in [4]–[6]. In particular, since we use (1)–(2) from [6] and the same parameter values, a convert algorithm implementation must yield the same results as with the *Finite Difference* (FD) implementation of [6]. This is demonstrated in Fig. 2 for p-i-n GaAs APDs (compare lines with open symbols). The figure also reports the experimental data from [14] (filled symbols).

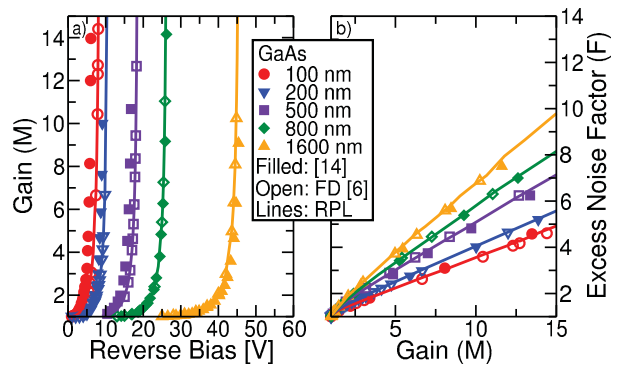


Fig. 2. (a) Gain vs. voltage and (b) excess noise factor vs. gain curves for GaAs p-i-n APDs of different thicknesses. The results obtained with the improved RPL algorithm (lines) are compared to the results of the Finite Difference implementation (open symbols, [6]) and with the experimental data from [14] (filled symbols).

B. Gain and noise in GaAs/AlGaAs staircase APDs

We now focus on staircase APDs. Fig. 3 shows the band diagram of the structure proposed in [15]: the top contact region is constituted by a 50-nm p^+ -GaAs layer ($N_A = 4 \cdot 10^{18} \text{ cm}^{-3}$), after that a 4.5- μm i-GaAs layer acts as the absorption region. The multiplication region consists of the periodic repetition of a 20-nm $i\text{-Al}_x\text{Ga}_{1-x}\text{As}$ (x from 0.0 to 0.45), a 25-nm $i\text{-Al}_{0.45}\text{Ga}_{0.55}\text{As}$ and a 35-nm i-GaAs layers and it is separated from the absorption region by a p-doped δ layer with nominal sheet concentration $\sigma = 2.5 \cdot 10^{12} \text{ cm}^{-2}$. The total length of the multiplication region is approximately 1 μm . On the bottom, a 200-nm n^+ -GaAs layer ($N_D = 2 \cdot 10^{18} \text{ cm}^{-3}$) separates the device from the n^+ -GaAs substrate.

Fig. 4 compares the gain and noise of our RPL algorithm with the experimental data from [15]: the experimental breakdown voltage is underestimated, but the trend of F vs. M is well reproduced.

C. Current waveforms

Current waveforms after generation of a single e-h pair are provided in Fig. 5. Plots (a), (b) consider the staircase structure excluding (a) or including (b) hole II; we observe that hole II

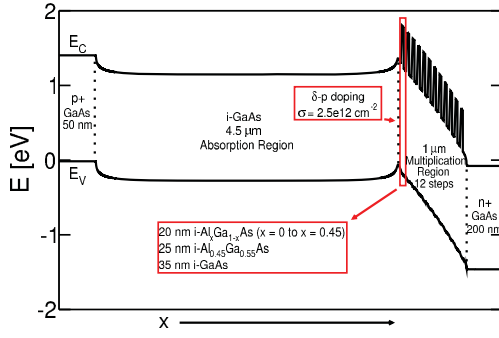


Fig. 3. Band diagram at equilibrium along the vertical direction of the staircase SAM-APD reported in [15].

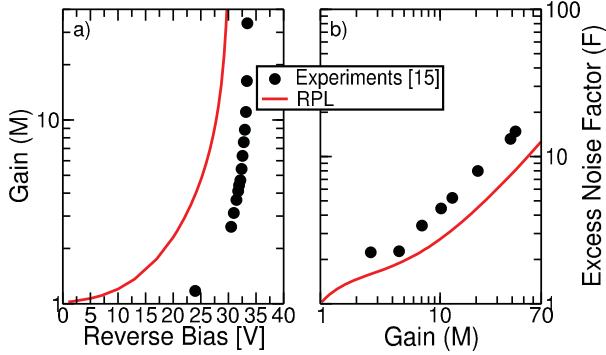


Fig. 4. (a) Gain vs. voltage and (b) excess noise factor vs. gain characteristics for the APD reported in [15]. The improved RPL algorithm (lines) is compared with the experimental data from [15] (filled symbols).

induces a long-lasting decaying tail in the current waveform, which becomes longer when the gain increases, whereas the current waveforms obtained when only electrons ionize have the same duration regardless of the gain. Plot (c) shows that the tail is slightly longer in p-i-n diodes. Notice that we consider constant voltage biasing, the *dynamic biasing* proposed in [16] would reduce the duration of these tails.

The Fourier transform of the waveforms normalized by the electron charge q gives the transfer function of the APD, since the *input signal* is the current pulse $q\delta(t)$ corresponding to the generation of the e-h pair. Sample profiles are reported in Fig. 6 and used to determine the -3dB bandwidth. We see that the inclusion of hole impact ionization reduces the bandwidth.

D. Exploration of the design space

To better visualize the advantages of a staircase structure compared to a p-i-n diode in terms of a gain/noise perspective, we compare in Fig. 7 the simulated M vs. voltage and F vs. M curves of the device in [15] (same as in Fig. 4) with a 1- μ m-thick GaAs p-i-n diode, i.e. same length of the multiplication region for both devices: the staircase structure shows significant gain also below the breakdown voltage and has a much lower associated noise.

The gain-bandwidth product (GBP, see Fig. 8) is almost constant [2] and improves for p-i-n APDs with thin intrinsic region. P-i-n and staircase diodes with the same width of

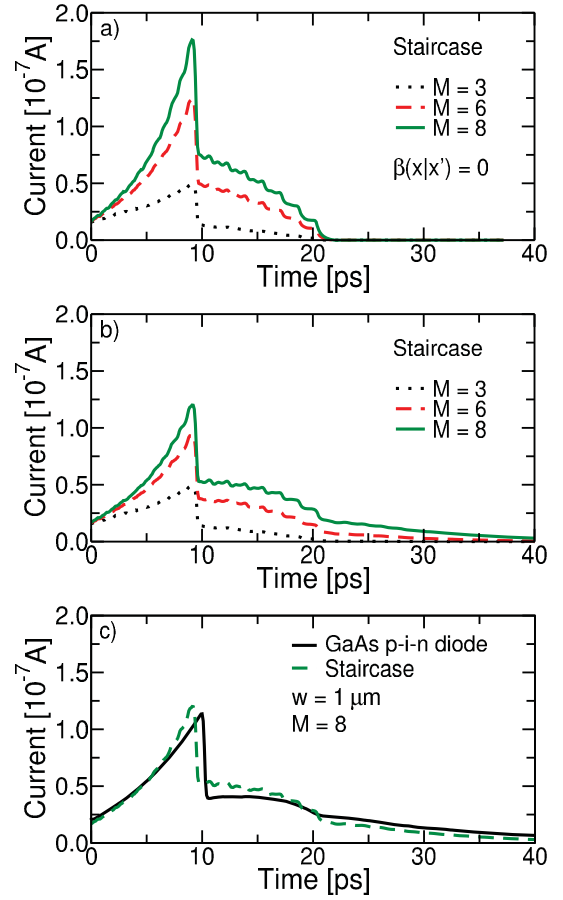


Fig. 5. Current waveforms at different RPL gains for the staircase SAM-APD of [15] obtained with the improved RPL algorithm (a) without or (b) with hole impact ionization. Notice that if holes do not ionize the duration of the current waveforms is independent of gain (plot (a)), while if holes ionize the current vs. time curves present a tail whose length becomes larger as the gain increases (plot (b)). (c) Current waveform of a 1- μ m-thick GaAs p-i-n diode (solid) and of the staircase SAM-APD (dashed), for $M = 8$. The 1- μ m GaAs p-i-n APD exhibits slightly longer hole II induced tails. Carriers move at a constant velocity $v_e = v_h = 10^7$ cm/s so that the transit time across the 1- μ m multiplication region is $T_R = 10$ ps.

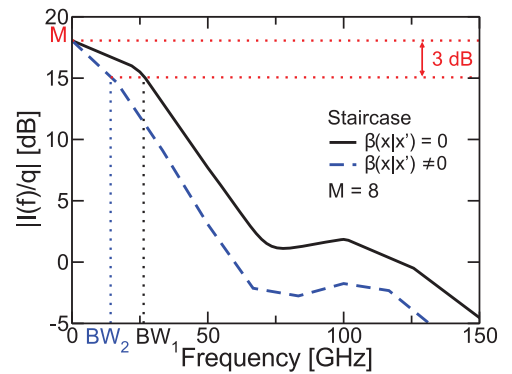


Fig. 6. Modulus of the Fourier transform of the current waveform of the staircase SAM-APD of [15] obtained excluding (solid) or including (dashed) hole II. The average gain is $M = 8 \approx 18$ dB, the -3dB bandwidths are, respectively, $BW_1 = 26$ GHz and $BW_2 = 14$ GHz.

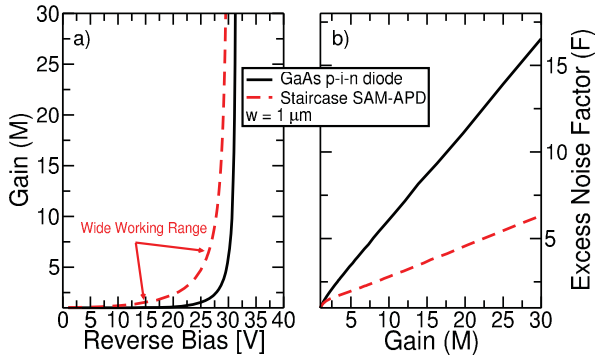


Fig. 7. (a) Gain vs. voltage and (b) excess noise factor vs. gain characteristics obtained with the improved RPL algorithm for a 1- μm -thick GaAs p-i-n APD and for the staircase SAM-APD reported in [15]. In the staircase SAM-APD we have an extended voltage range where a gain significantly larger than one is achieved.

the multiplication region have similar GBP. Note that the structure in [15] requires a significant electric field between the band discontinuities in order to obtain a significant gain. This results in large hole II which is detrimental for the bandwidth (see the long tail in Fig. 5, that implies a sharper decay in the frequency domain in Fig.6). This problem does not occur in other material systems (as for example in InAsSb systems [22]), where conduction band discontinuities are large compared to the energy gap of the material in which II takes place.

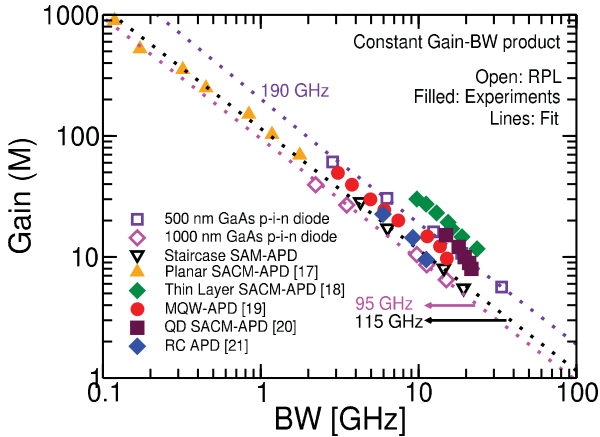


Fig. 8. Gain-bandwidth product of a 500 nm and a 1- μm -thick GaAs p-i-n diodes and of the staircase SAM-APD of [15] obtained with the RPL (open symbols). Filled symbols: experimental data for a planar [17] and a thin layer [18] separate, absorption, charge and multiplication (SACM), a Multi Quantum Well (MQW) [19], a quantum dot (QD) SACM [20] and a resonant cavity (RC) APDs [21] based on III-V compound semiconductors.

With the developed model we can thus explore the design space in terms of gain, noise and bandwidth. As an example, Fig. 9 compares the simulated bandwidth versus excess noise factor (at gain $M = 1, 2, 5, 10, 20$) with the ones determined with the RPL algorithm for different APD structures. We see that, consistently with the analysis in the previous pages, increased gains (obtained increasing the bias) result in smaller

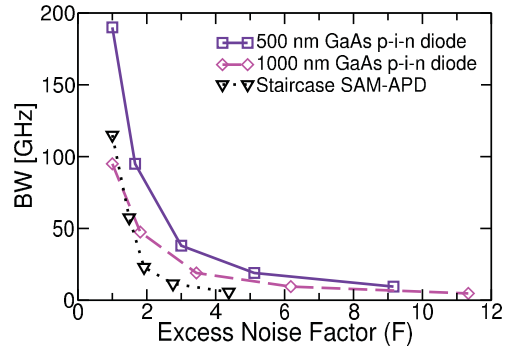


Fig. 9. Bandwidth versus excess noise factor at fixed gains (from left to right $M = 1, 2, 5, 10, 20$) of a 500 nm and a 1 μm -thick GaAs p-i-n diodes and of the staircase SAM-APD of [15] obtained with the RPL.

bandwidth and higher excess noise. For a given bandwidth, the staircase SAM-APD features lower excess noise compared with p-i-n diodes.

IV. CONCLUSION

The proposed improved RPL algorithm, coupled to the nonlocal model for impact ionization developed in [6], is capable to describe complex heterostructure APDs. It is shown that, as expected, staircase APDs are advantageous over p-i-n diodes in terms of excess noise, whereas the advantages in terms of gain-bandwidth product are limited unless hole II is significantly suppressed (Fig.6).

REFERENCES

- [1] R. J. McIntyre, "Multiplication noise in uniform avalanche diodes", IEEE Transactions on Electron Devices, vol. ED-13, no. 1, pp. 164-168, Jan. 1966. doi: 10.1109/T-ED.1966.15651.
- [2] R. B. Emmons, "Avalanche photodiode frequency response", Journal of Applied Physics, vol. 38, no. 9, pp. 3705-3714, Aug. 1967. doi: 10.1063/1.1710199.
- [3] F. Capasso, W.-T. Tsang, G. F. Williams, "Staircase solid-state photo-multipliers and avalanche photodiodes with enhanced ionization rates", IEEE Transactions on Electron Devices, vol. ED-30, no.4, pp. 381-390, Apr. 1983. doi: 10.1109/T-ED.1983.21132.
- [4] M. M. Hayat, W. L. Sargeant, B. E. A. Saleh, "Effect of dead space on gain and noise in Si and GaAs avalanche photodiodes", IEEE Journal of Quantum Electronics, vol. 28, no. 5, pp. 1360-1365, May 1992. doi: 10.1109/3.135278.
- [5] R. J. McIntyre, "A new look at impact ionization - part I: a theory of gain, noise, breakdown probability, and frequency response", IEEE Transactions on Electron Devices, vol. 46, no. 8, pp. 1623-1631, Aug. 1999. doi: 10.1109/16.777150.
- [6] C. Nichetti, A. Pilotto, P. Palestri, L. Selmi, M. Antonelli, F. Arfelli et al., "An improved nonlocal history-dependent model for gain and noise in avalanche photodiodes based on energy balance equation", IEEE Transactions on Electron Devices, vol. 65, no. 5, May 2018. doi: 10.1109/TED.2018.2817509.
- [7] Synopsis, "Sentaurus Device user guide", version L-2016.03, 2016.
- [8] M. M. Hayat, B. E. A. Saleh, "Statistical properties of the impulse response function of double-carrier multiplication avalanche photodiodes including the effect of dead space", IEEE Journal of Lightwave Technology, vol. 10, no. 10, pp. 1415-1425, Oct. 1992. doi: 10.1109/50.166785.
- [9] D. S. Ong, K. F. Li, G. J. Rees, J. P. R. David, "A simple model to determine multiplication and noise in avalanche photodiodes", Journal of Applied Physics, vol. 83, no. 6, pp. 3426-3428, Mar. 1998. doi: 10.1063/1.367111.

- [10] G. M. Williams, M. Compton, D. A. Ramirez, M. M. Hayat, A. S. Huntington, "Multi-gain-stage InGaAs avalanche photodiodes with enhanced gain and reduced excess noise", *IEEE Journal of the Electron Device Society*, vol. 1, no. 2, pp. 54-65, Feb. 2013. doi: 10.1109/JEDS.2013.2258072.
- [11] L.-A. Hamel, M. Julien, "Generalized demonstration of Ramo's theorem with space charge and polarization effects", *Nuclear Instruments and Methods in Physics Research Section A: Accelerators, Spectrometers, Detectors and Associated Equipment* vol. 597, pp. 207-211, Sep. 2008. doi: 10.1016/j.nima.2008.09.008.
- [12] C. Jacoboni, L. Reggiani, "The Monte Carlo method for the solution of charge transport in semiconductors with applications to covalent materials", *Review of Modern Physics*, vol. 55, issue 3, pp. 645-705, Jul. 1983. doi: 10.1103/revmodphys.55.645.
- [13] J. S. Ng, C. H. Tan, B. K. Ng, P. J. Hambleton, J. P. R. David et al., "Effect of Dead Space on avalanche speed", *IEEE Transactions on Electron Devices*, vol. 49, no. 4, Apr. 2002. doi: 10.1109/16.992860.
- [14] P. Yuan, K. A. Anselm, C. Hu, H. Nie, C. Lenox, A. L. Holmes et al., "A new look at impact ionization - part II: gain and noise in short avalanche photodiodes", *IEEE Transactions on Electron Devices*, vol. 46, no. 8, pp. 1632-1639, Aug. 1999. doi: 10.1109/16.777151.
- [15] J. Lauter, D. Protic, A. Forster, H. Luth, "AlGaAs/GaAs SAM-avalanche photodiode: an X-ray detector for low energy photons", *Nuclear Instruments and Methods in Physics Research A*, vol. 356, pp. 324-329, 1995. doi: 10.1016/0168-9002(94)01237-7.
- [16] M. M. Hayat, D. A. Ramirez, "Multiplication theory for dynamically biased avalanche photodiodes: new limits for gain bandwidth product", *Optics Express*, vol. 20, no.7, pp. 8024-8040, Mar. 2012. doi: 10.1364/OE.20.008024.
- [17] L. E. Tarof, J. Yu, R. Bruce, D. G. Knight, T. Baird, B. Oosterbrink, "High-frequency performance of separate absorption, grading, charge, and multiplication InP/InGaAs avalanche photodiodes", *IEEE Photonics Technology Letters*, vol. 5, no. 6, pp. 672-674, Jun. 1993. doi: 10.1109/68.219706.
- [18] K. A. Anselm, H. Nie, C. Hu, C. Lenox, P. Yuan, G. Kinsey et al., "Performance of thin separate absorption, charge, and multiplication avalanche photodiodes", *IEEE Journal of Quantum Electronics*, vol. 34, no. 3, pp., 482-490, Mar. 1998. doi: 10.1109/3.661456.
- [19] K. Makita, I. Watanabe, M. Tsuji, K. Taguchi, "150 GHz GB-product and low dark current InAlGaAs quaternary well superlattice avalanche photodiodes", *Proceedings IOOC-95,1995*, p. 36, paper TuB2-1.
- [20] P. Yuan, O. Baklenov, H. Nie, A. L. Holmes Jr., B. G. Streetman, J. C. Campbell, "High-speed and low-noise avalanche photodiode operating at 1.06 μm ", *IEEE Journal of Selected Topics in Quantum Electronics*, vol. 6, no. 3, pp. 422-425, May/Jun. 2000. doi: 10.1109/2944.865097.
- [21] H. Nie, K. A. Anselm, C. Hu, B. G. Streetman, J. C. Campbell, "High-speed, low-noise resonant-cavity avalanche photodiodes", *Proceedings LEOS'96*, Nov. 1996. doi: 10.1109/LEOS.1996.565298.
- [22] M. Ren, S. Maddox, Y. Chen, M. Woodson, J. C. Campbell, S. Bank, "AlInAsSb/GaSb staircase avalanche photodiodes", *Applied Physics Letters*, vol. 108, no. 8, pp. 081101-1-081101-4, Feb. 2016. doi: 10.1063/1.4942370.